J. Eng. Technol. Sci., Vol. 53, No. 4, 2021, 210407

Development of Laboratory-scale Lamb Wave-based Health Monitoring System for Laminated Composites

Leonardo Gunawan*, Muhammad Hamzah Farrasamulya, Andi Kuswoyo & Tatacipta Dirgantara

Faculty of Mechanical and Aerospace Engineering, Institut Teknologi Bandung,
Jalan Ganesha No. 10, Bandung 40132, Indonesia
*E-mail: gun@ftmd.itb.ac.id

Highlights:

- Development of a structural health monitoring (SHM) system for laminated composites.
- Experimental investigation of a damaged laminated composite plate by means of the SHM system.
- Image reconstruction of damage by means of SHM detection results.

Abstract. This paper presents the development process of a laboratory-scale Lamb wave-based structural health monitoring (SHM) system for laminated composite plates. Piezoelectric patches are used in pairs as actuator/sensor to evaluate the time of flight (TOF), i.e. the time difference between the transmitted/received signals of a damaged plate and those of a healthy plate. The damage detection scheme is enabled by means of evaluating the TOF from at least three actuator/receiver pairs. In this work, experiments were performed on two GFRP plates, one healthy and the other one with artificial delamination. Nine piezoelectric transducers were mounted on each plate and the detection of the delamination location was demonstrated, using 4 pairs and 20 pairs of actuators/sensors. The combinations of fewer and more actuators/sensor pairs both provided a damage location that was in good agreement with the artificial damage location. The developed SHM system using simple and affordable equipment is suitable for supporting fundamental studies on damage detection, such as the development of an algorithm for location detection using the optimum number of actuator/sensor pairs.

Keywords: *composite; damage introduction; Lamb wave; piezoelectric; SHM.*

1 Introduction

Composite structures are increasingly used in broad applications, e.g. automotive, construction, aerospace and biomedical applications [1]. In the past decades, composites transformed from being used for secondary structures into primary structures applications to bear main loads exerted to the system. However, understanding the behaviors of composites in load-bearing structures remains a

Received July 16th, 2020, Revised December 11th, 2020, Accepted for publication March 12th, 2021.
 ISSN: 2337-5779,
DOI: 10.5614/j.eng.technol.sci.2021.53.4.7

challenging task. Composite strength may be reduced significantly after damage, even from low-velocity impacts [2].

Failure analyses of composites have been conducted through various numerical methods [3-5] and experimental tests [6,7]. However, often the existence of damage may only be known after the damage has occurred. The works on damage analysis concerning structural strength have always been in line with the development of non-destructive evaluation (NDE) methods [8-10] or with the emergence of SHM techniques [11,12].

In particular hardly visible damage, e.g. barely visible impact damage (BVID), is one of the main concerns in the development of damage detection systems [13]. Concerning life after damage, the structure may experience damage growth under cyclic/fatigue loading, leading to a life limit decline [14]. SHM must be conducted regularly to structures in order to assess their integrity during their operational life cycle. The NDE technique causes minimum disturbance to the structural serviceability during the inspection process. Moreover, in composites, NDE can give critical surface or volume information concerning damage such as delamination, matrix cracking, or fiber breakage. Recent progress in the development of SHM systems has sought the use of in-situ piezoelectric sensors [15].

In contrast with conventional NDE systems, which have a drawback in the determination of damage initiation time in that they require a particular time for inspection [12], in-situ SHM systems provide active, continuous, real-time monitoring of the damage initiation and progression. The attached piezoelectric transducers are critical parts of the SHM system. They enable an evaluation/inspection process without the need for scheduled out-of-service testing. However, to complete the SHM system, a voltage generator system also needs to be included as part of the structure. The advancement of multifunctional structures [16] sought beneficial insight into work towards in-situ SHM systems. Research on self-charging piezoelectric-based structures [17-19] has increased significantly. Future studies are expected to enable self-charging SHM systems.

The Lamb wave-based system is a leading state-of-the-art NDE technique. Often, piezoelectric transducers are utilized to generate/detect waves. The damage location algorithm is based on the time difference between the Lamb waves generated at one point and detected at another point in a healthy plate and a damaged plate. In the healthy plate, the detected signal at the second point contains only waves travelling directly from the first point. In contrast, in the damaged plate the detected signal contains waves travelling directly from the first point and waves reflected from damage [11].

This paper presents the development of an in-situ Lamb wave-based SHM system for the evaluation of damage to composite structures. The main target was to enable an efficient yet straightforward piezoelectric transducer system as a fundamental component of the SHM system. The design and development of the proposed SHM system are discussed in Section 2. Then, a brief introduction of Lamb waves, piezoelectric transducers and the damage localization procedure is presented. Finally, the results of the verification of the SHM system concerning the delamination of a composite plate are given.

2 Lamb Wave-based SHM System

2.1 Lamb Wave Overview

Lamb [15] emphasized the importance of mathematical modeling for vibrations-related cases in seismology concerning elastic layers with various densities and elasticities. Lamb waves, also known as plate waves, were first observed in homogeneous isotropic materials. The waves travel in a solid plate through symmetrical or anti-symmetrical motion to a neutral axis. Symmetric Lamb waves, so-called S waves, represent longitudinal waves, while anti-symmetric waves, so-called A waves, represent transversal waves [15].

Worlton [20] performed one of the earliest ultrasonic tests using Lamb waves to investigate abnormal grain growth within thin metal strips. Since then, various studies on non-contact Lamb waves-based structural inspection methods have been conducted, e.g. by exposing the surface of a plate to a piezoelectric transducer probe [21-23]. Concerning structural testing, Lamb waves exhibit a dispersive characteristic, i.e. the velocity of the waves is dependent on the frequency. However, within particular frequency ranges, the so-called non-dispersive regions, the velocity is independent of the frequency, as depicted in Figure 1. This property can be used for testing purposes as the velocity can be set constant within a frequency range [24].

As reviewed by Diamanti & Soutis [11], in line with the growing attention towards the development of smart structures, small transducers have been implemented to establish an attached inspection system. One of the main benefits of this scheme is the possibility to generate much more frequent or even continuous waves, enabling a continuous monitoring scheme, the so-called structural health monitoring (SHM), instead of periodic scheduled inspection [12].

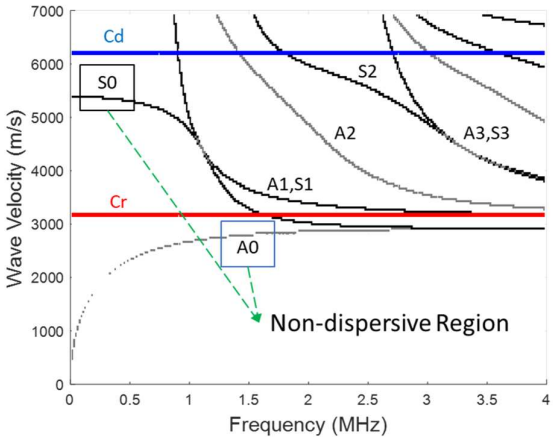

Figure 1 Thin aluminum plate dispersion curves for various symmetric and anti-symmetric waves (compiled by the authors).

2.2 Piezoelectric Actuators and Sensors

Lamb wave-based SHM applications utilize the piezoelectric material's electromechanical coupling to generate/detect electrical fields and mechanical strains. Piezoelectric constitutive properties are commonly divided into two forms, i.e. stress-charge and strain-charge forms. The strain-charge form [25] is expressed in a matrix Eq. (1). $\mathbf{E_{iJMn}}$ is a 9 x 9 matrix depicting the electromechanical constitutive properties of the piezoelectric material. C is known in mechanical problems as the elasticity matrix. The electromechanical coupling constant, e, represents the link between the mechanical load and the electric potential. Meanwhile, the permittivity, ε^S, defines the electric capacitance of the material.

$$\mathbf{E_{iJMn}} = \begin{bmatrix} \mathbf{C} & -\mathbf{e^t} \\ (6x6) & (6x3) \\ \mathbf{e} & \boldsymbol{\varepsilon^S} \\ (3x6) & (3x3) \end{bmatrix} \tag{1}$$

The piezoelectric materials as actuators are given an electrical input; hence, electricity fields are generated and mechanical strains are created [25]. Periodic mechanical strains propagate through the structure so elastic waves are created. These mechanical strains, vice versa, generate electrical fields and are detected by the piezoelectric sensors as electric potential. Piezoelectric patches can be arranged with an array of electrodes on a structure, i.e. an interdigital transducer, or placed so that the patches sandwich the structure, i.e. a wafer transducer [11].

In the present work, an interdigital transducer arrangement, as illustrated in Figure 2, was used to detect the damage in a composite laminate plate.

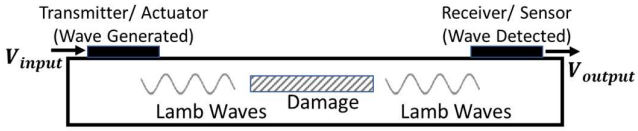

Figure 2 Arrangement of an interdigital transducer with piezoelectric patches on the surface of a plate.

2.3 Damage Localization Method

In the present work, a frequency regime in which the Lamb waves could propagate with little dispersion was applied. Thus, the velocity of the wave generated by the piezoelectric patch was easier to verify in the control (healthy) structure. The so-called variable time of flight (TOF) between two known separated sensors can be measured by an oscilloscope [26].

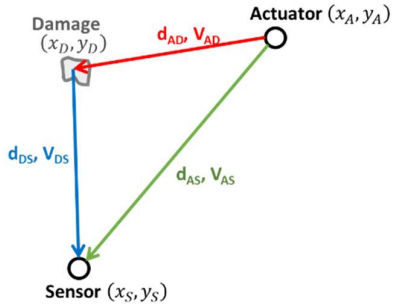

Figure 3 Wave propagation process.

Figure 3 illustrates the process of wave propagation in an infinite plate with damage. The symbols x and y represent the in-plane coordinates, while the subscripts D, S, and A denote the damage, sensor, and actuator, respectively. In addition, the symbols d and v represent the shortest distance and wave propagation velocity between two coordinates, respectively. The TOF is defined as the time difference between the actuator-sensor's direct wave and the reflected wave coming from the damage. By defining t as the time traveled by the wave between two coordinates, the TOF can be expressed as in Eq. (2):

$$TOF = (t_{AD} + t_{DS}) - t_{AS} \tag{2}$$

Using the distance, velocity and time relation one can expand this expression as in Eq. (3):

$$TOF = \left(\frac{d_{AD}}{v_{AD}} + \frac{d_{DS}}{v_{DS}}\right) - \frac{d_{AS}}{v_{AS}} \tag{3}$$

where

$$\begin{aligned} d_{AD} &= \sqrt{(x_D - x_A)^2 + (y_D - y_A)^2} \\ d_{AS} &= \sqrt{(x_S - x_A)^2 + (y_S - y_A)^2} \\ d_{DS} &= \sqrt{(x_S - x_D)^2 + (y_S - y_D)^2} \end{aligned} \tag{4}$$

The solution in Eq. (4) is not unique since the distances are unknown except the distance between the actuator and the sensor, d_{AS}. In other words, there exist multiple damage locations (loci), which may further be deduced to depict the most probable solution. A locus is shaped like an ellipse, as shown in Figure 4. Additional loci must be created (i.e. involving new actuator-sensor pairs) to find the intersection of loci; thus, a unique solution is obtained. Eventually, at least three loci should be used to reduce the loci into one damage location.

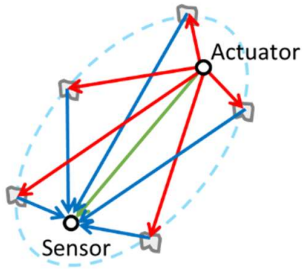

Figure 4 Loci of possible damage with similar TOF value.

The workflow to obtain a damage location prediction by means of the TOF calculation is presented in Figure 5. First, an actuator-sensor pair creates and detects a Lamb wave pulse in a healthy plate as reference. Hilbert transformation is then applied to the time response to determine the energy envelope of the signal. Then, auto-correlation values of the energy envelope of the time response are determined. When a plate gets damaged and the same procedure is repeated, auto-correlation values of the damaged plate's time response can be obtained. The highest difference between the two auto-correlation values indicates the reflection from the damage and the time when the highest auto-correlation values occur is interpreted as the TOF.

A typical voltage response and energy envelope measured by the sensor for a healthy and a damaged plate are shown in Figure 6. In this case, the actuator creates a sinusoidal wave multiplied by the Hanning window function. Hence, the input signal is in pulse form and is not continuous. It can be seen that when

the first Lamb wave was detected (at around 30 microseconds), both sensors on the healthy and the damaged plate had almost exactly the same time response. However, it can be seen that after the first wave there were differences between both sensors. On the damaged plate, the sensor detected another oscillation pattern at around 70 microseconds. This indicates the presence of damage or inclusion that does not exist in the healthy plate. After 70 microseconds, both time responses contain the same pulses, which indicates reflections from objects in the healthy and damaged plates and hence are not of interest to the analysis. Figure 7 depicts the correlation coefficients between the two plates and their variance, which is used to determine the TOF value.

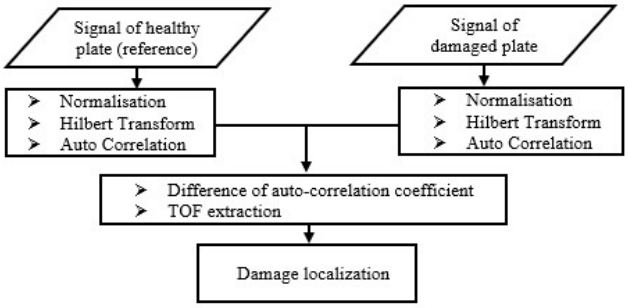

Figure 5 Workflow of damage localization.

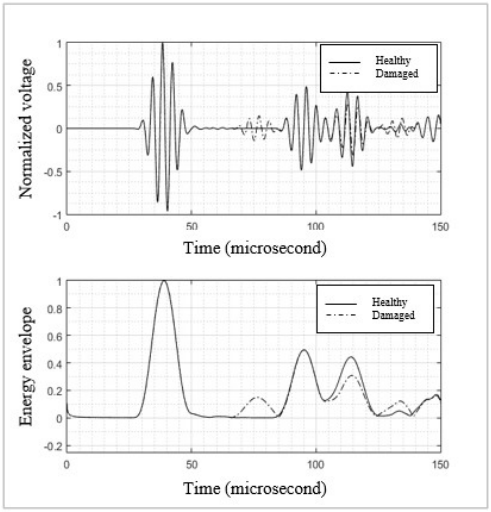

Figure 6 Typical voltage responses (top) and energy envelope (bottom) measured by the sensors.

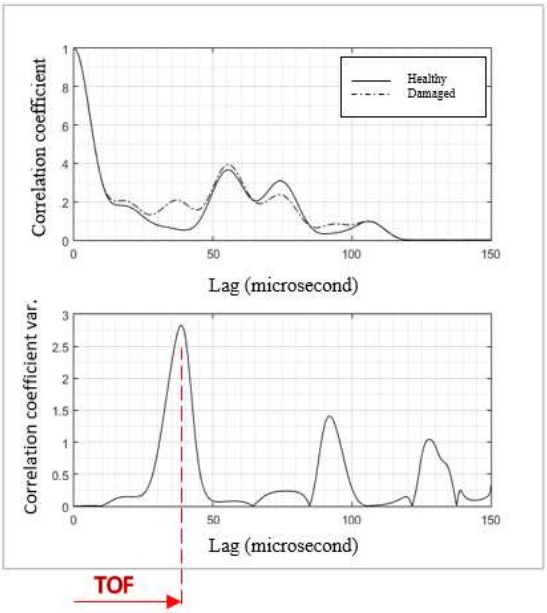

Figure 7 Typical correlation coefficients (top) and correlation coefficients variance (bottom) between the healthy and damaged plates.

3 Experimental Set-up

3.1 GFRP Plate

A thin laminated composite plate was evaluated in the present work, instrumented with piezoelectric patches to conduct an SHM test concerning damage. The propagation of Lamb waves in a laminated composite is much more complicated than in an isotropic plate. The volume fractions and layup sequence influence the wave's anisotropy characteristic and dispersive behavior [20].

A quasi-isotropic configuration $[0/45/-45/90]_S$ was chosen as stacking sequence to avoid this directional dependency. The specimen with this stacking configuration was manufactured using glass fiber (plain-woven) and a resin-based matrix. Two specimens were manufactured. The first specimen was a 44 x 40 x 0.127 cm GFRP plate, as depicted in Figure 8, representing a healthy structure. The second one was a similar plate but with the inclusion of an aluminum coin with 5 cm diameter and 0.3 mm thickness in the middle of the plate to represent a damaged plate. The location and a sample of the inclusion are shown in Figures 9 and 10, respectively.

3.2 Transducers Selection and Installation

Disc-shaped PZT-5H transducers were used as actuators and sensors. Each transducer had a diameter of 15 mm and a thickness of 1 mm, as depicted in Figure 11. This transducer is commonly utilized as an actuator/sensor for micro electro mechanical system (MEMS) applications. It has strong electromechanical couplings and stiffness of the same order as common metals like aluminum. In addition, disc-shaped transducers are cheap and readily available in the market.

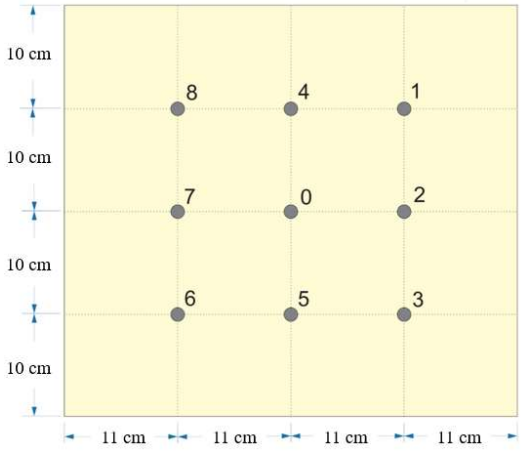

Figure 8 The composite plate with 9 distributed piezoelectric transducers.

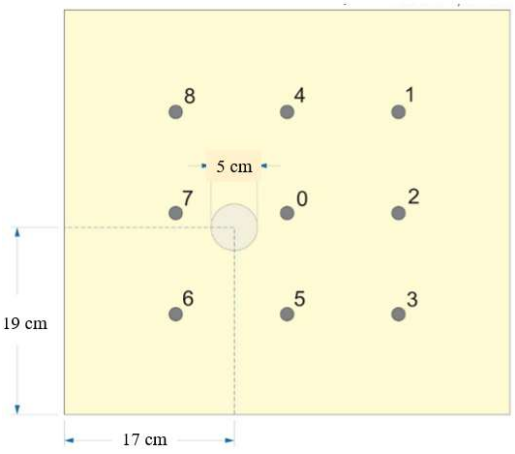

Figure 9 Location of the aluminum inclusion within the laminated composite plate with 9 distributed piezoelectric transducers.

The transducers were attached to the surface of the plates using an epoxy-resin based adhesive material. The transducer network was created by distributing nine transducers on both the healthy and the damaged plate, as shown in Figures 8 and 9. The transducers on both the healthy and the damaged plate are denoted by the numbers 0 to 8. The transducer distribution represents four quadrants in a polar coordinate system with the middle one, transducer 0, as the center.

Figure 10 The aluminum inclusion.

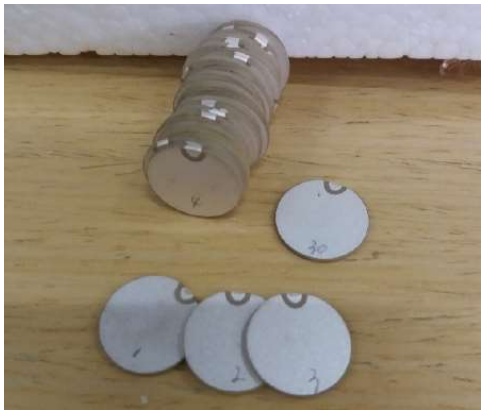

Figure 11 The disc-shaped PZT-5H transducers.

3.3 SHM System Set-up

The primary system instrumentation consists of: (a) a charge amplifier to convert the electrical charge produced by the sensor to voltage; (b) a digital oscilloscope to record and visualize the variation of voltage versus time; (c) an arbitrary signal generator (AFG) to produce the driving voltage for the actuator. Additional system features such as analog and digital filters were used to remove noise or signals outside of the designed value. An illustration of the SHM system is shown in Figure 12. The AFG was connected to the transducer, defined as actuator, hence providing an input voltage to the actuator. For output voltage reading, the transducer, defined as sensor, was connected to a charge amplifier. The charge

amplifier and the AFG were connected to the oscilloscope; thus, the input and output voltages could be displayed.

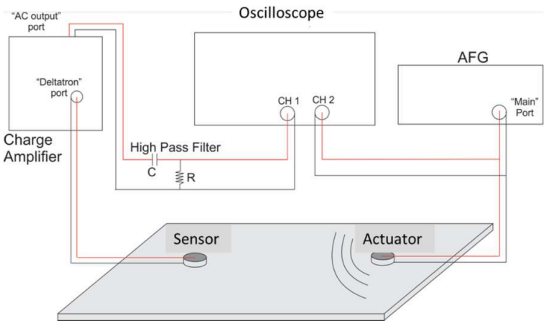

Figure 12 Illustration of the present piezoelectric Lamb wave-based SHM system.

Figure 13 shows the experimental set-up, which includes a charge amplifier, a digital oscilloscope, and the AFG. The charge amplifier was a B&K 2525 device with an output gain up to 20dB. The digital oscilloscope used here was a RIGOL DS1102E device with 16 channels and up to 100 MHz bandwidth. An essential feature for the selection of the oscilloscope is its data transferability. A USB host with simple integration to a computer unit is highly beneficial for data processing. A GW-Instek AFG3081 was used in the present work as the AFG. This AFG has a maximum frequency of 80 MHz and peak-to-peak voltage up to 20 Volt. The AFG was operated at the Lamb wave frequency for thin flat plates, i.e. around 100-500 kHz, at the maximum voltage amplitude.

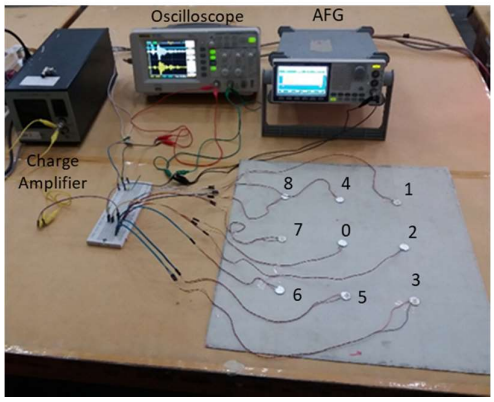

Figure 13 Experimental set-up of the SHM system (top part, from left to right: the charge amplifier, digital oscilloscope and AFG).

4 Damage Detection Test

4.1 Velocity Directional Dependency Evaluation

As shown in Figure 8, the transducers formed four quadrants in a polar coordinate system with a transducer in the middle (transducer 0) as the center. By defining transducer 0 as actuator while the remaining ones act as sensors, eight actuator/sensor pairs were enabled. The wave velocity could be verified by evaluating the arrival times of the first wave to each sensor. In the present case, the excitation frequency was varied from 230 kHz to 260 kHz.

A relatively uniform velocity distribution was obtained for all pairs, with an average value of 3459 m/s. This velocity indicates that the initial assumption of velocity directional independency of the wave traveling in the quasi-isotropic plate is still acceptable. A frequency selection that does not produce a significant difference implies that the frequency selected is within the dispersion curves' non-dispersive region.

4.2 Voltage Signals of Healthy and Damaged Plates

The main excitation frequency applied to actuator was 240 kHz. Figure 14 shows the recorded voltage signals of the 8-1 transducer pair for both the healthy and the damaged plate. The waves' average velocity was considered to verify the measured responses. As depicted in Figure 8, the shortest distance between actuator 8 and sensor 1 was 22 cm. Hence, the time traveled by the waves from actuator 8 to sensor 1 was around 60 microseconds, i.e. an average wave velocity of 3459 m/s. This estimation verifies the response shown in Figure 14, in which the first oscillation patterns start at around 60 microseconds for both the healthy and the damaged plate. It should be noted that there were small oscillation patterns at the beginning of the measurements on both plates. These patterns represent some noise and do not represent the measured response and thus can be neglected.

A significant difference was observed in the damaged plate's response compared to the healthy plate. The measured response from the healthy plate shows that the second wave started at around 120 microseconds. However, on the damaged plate, some disturbances occurred at about 90-110 microseconds. In this case, the red-circled area indicates the presence of a damage-reflected wave. It can be seen in Figure 15 that the region that displayed a damage-reflected wave resulted in another peak of energy.

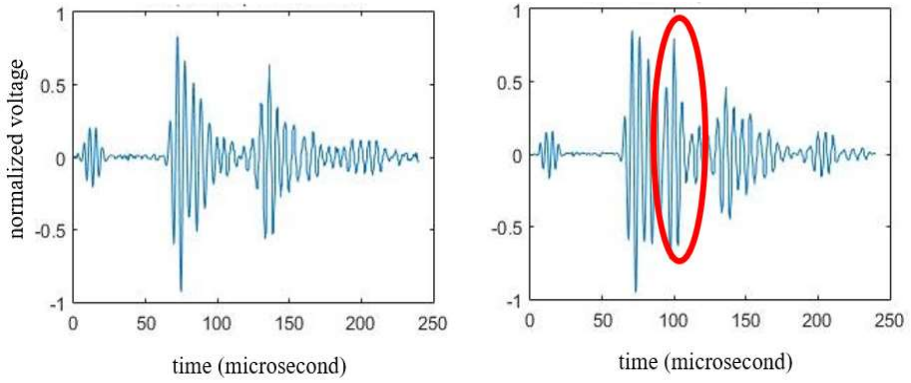

Figure 14 Recorded voltage signals of the 8-1 actuator-sensor combination for the healthy plate (left) and the damaged plate (right).

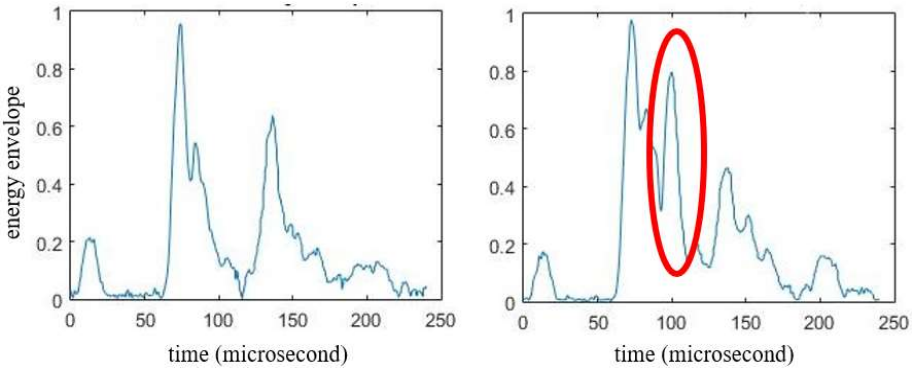

Figure 15 Energy envelope curves of the 8-1 actuator-sensor combination for the healthy plate (left) and the damaged plate (right).

The TOF value can be readily obtained and used as input for the imaging algorithm by using the correlation coefficient difference. Figure 16 shows the correlation coefficients for the healthy and the damaged plate and their variance for the 8-1 actuator-sensor pair.

The TOF values were extracted from the maximum variances of the correlation coefficients. For the image reconstruction process, from the four actuator-sensor pairs, the three maximum variances from each pair were applied to reconstruct the locus of possible damage. The details of this process are discussed in Section 5.

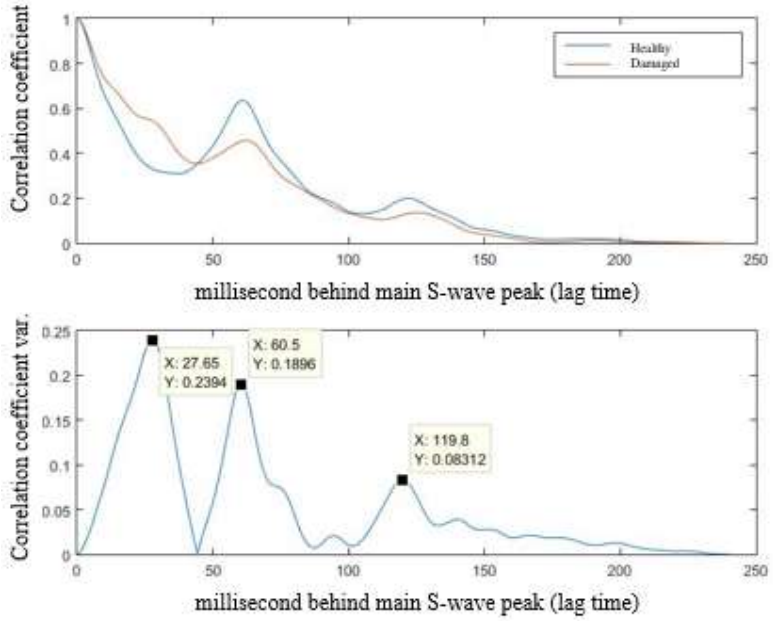

Figure 16 Correlation coefficients (top) and correlation coefficient variance (bottom) measured from the 8-1 actuator-sensor combination.

5 Damage Location Imaging

One of the most effective ways to communicate the SHM sensing activity result is by creating an image that shows where the damage is most probably located. This can be done by creating a digital image consisting of a finite set of pixels. Each of them corresponds to a limited volume located at specific coordinates within the structure. Based on the initial actuator and sensor coordinates, using the same equation as applied in the calculation of damage loci, each pixel in this image will be assigned a new TOF value obtained by assuming that that pixel is the center of a damaged area.

This set of newly computed TOF values is then compared to the actual TOF values obtained using the signal processing method. Pixels whose computed TOF has a small difference with the actual TOF implies that the volume it represents in the existing structure is located close to the real damage. How small that difference is, is quantified by a new variable called the damage index, which is visually shown by color variation.

In the present work, a different algorithm was developed to combine images produced by other actuator/sensor pairs. In this phase, the ellipses' intersection is emphasized by the increase of the damage index of the pixels surrounding it. As more ellipses are used, more crossings are created, where the highest intersection area can be inferred as the most probable damage location.

5.1 Ellipse Image Generation (4 Pairs)

The ellipses for the case of four actuator/sensor pairs are depicted in Figure 17. In this case, one ellipse was generated from each pair. The ellipse was reconstructed from the TOF value concerning the first peak of the correlation coefficient variance. Hence, four ellipses were created from four different actuator/sensor combinations. Piezoelectric patches number 8 and 5 were used as actuators, while patches number 1 and 2 were used as sensors. It can be seen that each ellipse follows the direction of the activated actuator and sensor. As an example, the ellipse created from the 8-1 combination was elongated in the x-direction. The intersections of the four ellipses depicts the area that has the highest probability of damage.

In the present case, all four ellipses may not intersect in one point, but their intersections localize the damaged area. As displayed in Figure 17, the ellipses' intersections agreed well with the designed damage location. Despite this fact, during the data extraction for TOF (correlation coefficients), there is a possibility that multiple peaks occur at the beginning, which may cause misinterpretation of the results. Therefore, in the next step of the experiment more combinations were utilized. It was expected that with more combinations the most probable damage location could be better justified by taking the ellipses' intersection point with the highest intensity.

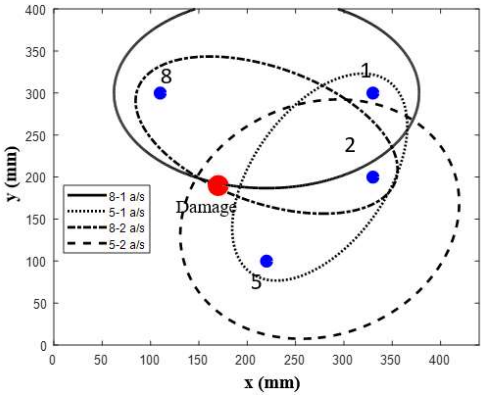

Figure 17 Reconstructed ellipses of the 8-1, 5-1, 8-2, 5-2 actuator/sensor pairs.

5.2 Ellipse Image Generation (20 Pairs)

By employing multiple actuator/sensor pairs, the uncertainty of the damage location can be reduced. In this study, 20 actuator/sensor pairs were used for further investigation. The experimental set-up for both the healthy and the damaged plate is shown in Figure 18. The actuator/sensor pairs are depicted in Table 1.

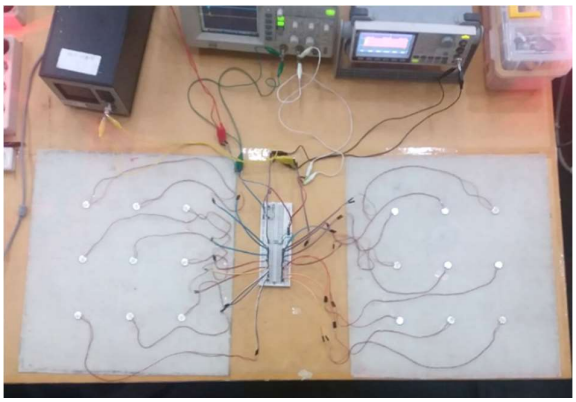

Figure 18 Final experimental set-up.

A particular TOF extraction procedure was used, where only the highest correlation difference peak was chosen as the TOF value. The ellipse images generated from the first ten pairing combinations are displayed in Figure 19. It can be seen that each pair had a different region of focus. However, by combining all ellipses, intersecting regions could be defined.

Table 1 20 Pairing Actuator-Sensor Combinations

Actuator	Sensor	Pair No.	Actuator	Sensor	Pair No.
1	0	1	4	0	13
	4	2		7	14
	5	3		8	15
	8	4			
2	0	5	5	0	16
	4	6		4	17
	5	7		6	18
	8	8			
3	0	9	6	7	19
	4	10		8	20
	5	11			
	6	12			

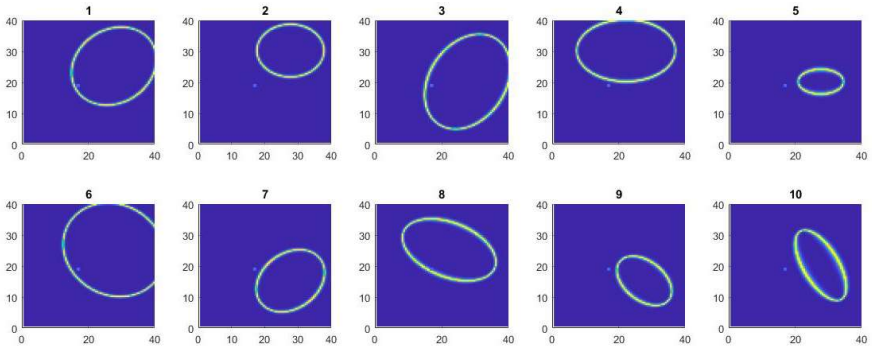

Figure 19 Ellipses generated from the first 10 actuator/sensor pairs.

The resulting ellipses from the 20 pairs were connected as shown in Figure 20. Image smoothing was conducted; the resulting image is also shown. In this phase, there was a group of intersecting loci near the damage location. From the smoothed image, the area with the highest color intensification could be seen at around x = 17 cm and y = 19 cm; thus, it was well verified with the designed damage location shown in Figure 9. In a future work, optimum locations of the piezoelectric actuators/sensors will be determined to provide maximum area coverage [27,28].

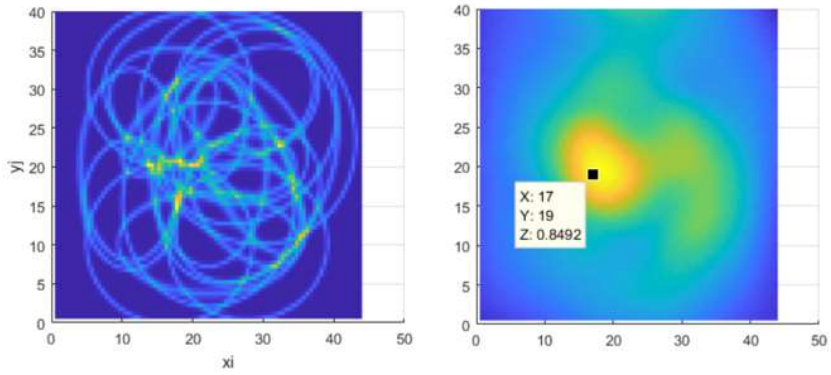

Figure 20 Ellipses intersection of 20 actuator/sensor pairs (left); smoothing result of the image (right).

6 Conclusion

A Lamb wave-based SHM system was developed. The system was set up at laboratory scale. Investigation on a healthy and a damaged composite plate was

conducted. Piezoelectric transducers were utilized as actuators and sensors to provide TOF information on the propagating wave.

An inclusion was applied to simulate delamination of the composite plate. Apparent differences were found between the signals recorded for the healthy and the damaged plate. Additional reflected waves indicate the existence of damage in the composite plate. By employing digital imaging the locus or ellipse of each actuator/sensor pair could be displayed. Visualization of the damage location based on the intersections of the ellipses was enabled. The accuracy and consistency of the present system were validated by varying the number of actuator/sensor pairs.

It is necessary to consider the optimal placement of the actuators/sensors in the SHM system. In the present case, a relatively small structure was observed. However, in practice much larger structures, e.g. aircraft structures, need to be evaluated. Hence, the wave traveling coverage area from the actuator to the sensor needs to be as large as possible.

Acknowledgement

This research was funded by *Kementerian Riset, Teknologi dan Pendidikan Tinggi, Indonesia* under the PDUPT 2019 scheme, which is greatly acknowledged. The authors would also like to thank the Royal Academy of Engineering, UK for providing ideas and thoughts through the Newton Fund, Industry-Academia Partnership Programme.

References

[1] Rajak, D.K., Pagar, D.D., Kumar, R. & Pruncu, C.I., *Recent Progress of Reinforcement Materials: A Comprehensive Overview of Composite Materials*, Journal of Materials Research and Technology, **8**(6), pp. 6354-6374, 2019.

[2] Soutis, C., *Carbon Fibre Reinforced Plastics in Aircraft Structures*, Materials Science and Engineering A, **412**(1-2), pp. 171-176, 2005.

[3] Senthil, K., Arockiarajan, A., Palaninathan, R., Santhosh, B. & Usha, K.M., *Defects in Composite Structures: Its Effects and Prediction Methods – A Comprehensive Review*, Composite Structures, **106**, pp. 139-149, 2013.

[4] Abdullah, N.A., Curiel-Sosa, J.L., Taylor, Z.A., Tafazzolimoghaddam, B., Vicente, J.L.M. & Zhang, C., *Transversal Crack and Delamination of Laminates Using XFEM*, Composite Structures, **173**, pp. 78-85, 2017.

[5] Abdullah, N.A., Akbar, M., Wirawan, N. & Curiel-Sosa, J.L., *Assessment on Cracked Composites Interaction with Aeroelastic Constraint by Means of XFEM*, Composite Structures, **229**, 111414, 2019.

[6] Shah, S.Z.H., Karuppanan, S., Megat-Yusoff, P.S.M. & Sajid, Z., *Impact Resistance and Damage Tolerance of Fiber Reinforced Composites: A Review*, Composite Structures, **217**, pp. 100-121, 2019.

[7] Andrew, J.J., Srinivasan, S.M., Arockiarajan, A. & Dhakal, H.N., *Parameters Influencing the Impact Response of Fiber-reinforced Polymer Matrix Composite Materials: A Critical Review*, Composite Structures, **224**, 111007, 2019.

[8] Rehman, S.K.U., Ibrahim, Z., Memon, S.A. & Jameel, M., *Nondestructive Test Methods for Concrete Bridges: A Review*, Construction and Building Materials, **107**, pp. 58-86, 2016.

[9] Yang, R., He, Y. & Zhang, H., *Progress and Trends in Nondestructive Testing and Evaluation for Wind Turbine Composite Blade,* Renewable and Sustainable Energy Reviews, **60**, pp. 1225-1250, 2016.

[10] Towsyfyan, H., Biguri, A., Boardman, R. & Blumensath, T., *Successes and Challenges in Non-destructive Testing of Aircraft Composite Structures*, Chinese Journal of Aeronautics, 2019.

[11] Diamanti, K. & Soutis, C., *Structural Health Monitoring Techniques for Aircraft Composite Structures*, Progress in Aerospace Sciences, **46**, pp. 342-352, 2010.

[12] Tuloup, C., Harizi, W., Aboura, Z., Meyer, Y., Khellil, K. & Lachat, R., *On the Use of In-situ Piezoelectric Sensors for the Manufacturing and Structural Health Monitoring of Polymer-matrix Composites: A Literature Review*, Composite Structures, **215**, pp. 127-149, 2019.

[13] Talreja, R. & Phan, N. *Assessment of Damage Tolerance Approaches for Composite Aircraft with Focus on Barely Visible Impact Damage*, Composite Structures, **219**, pp. 1-7, 2019.

[14] Molent, L. & Haddad, A., *A Critical Review of Available Composite Damage Growth Test Data Under Fatigue Loading and Implications for Aircraft Sustainment*, Composite Structures, **232**, 111568, 2020.

[15] Lamb, H., *On Waves in an Elastic Plate*, Proceedings of the Royal Society of London, **114**, 8, 1917.

[16] Ferreira A.D.B., Nvoa, P.R. & Marques, A.T., *Multifunctional Material Systems: A State-of-the-art Review*, Composite Structures, **151**, pp. 3-35, 2016.

[17] Tsushima, N. & Su, W., *Concurrent Active Piezoelectric Control and Energy Harvesting of Highly Flexible Multifunctional Wings*, Journal of Aircraft, **54**(2), pp. 724-36, 2017.

[18] Erturk, A. & Inman, D.J., *Piezoelectric Energy Harvesting*, 1st ed., John Wiley & Sons, Ltd., 2011.

[19] Akbar, M. & Curiel-Sosa, J.L., *An Iterative Finite Element Method for Piezoelectric Energy Harvesting Composite with Implementation to Lifting Structures Under Gust Load Conditions*, Composite Structures, **219**, pp. 97-110, 2019.
[20] Worlton, D.C., *Ultrasonic Testing with Lamb Waves*, Technical Report HW-45649 (Del.), DOE's Office of Scientific and Technical Information (OSTI), 1956.
[21] Lehfeldt, E. & Hoeller, P., *Lamb Waves and Lamination Detection*, Ultrasonics, **5**(4), pp. 255-257, 1967.
[22] Demer, L.I. & Fentnor, L.H., *Lamb Wave Techniques in Nondestructive Testing*, International Journal of NDT, **1**, pp. 251-283, 1969.
[23] Farlow, R. & Hayward, G., *Real-Time Ultrasonic Techniques Suitable for Implementing Non-Contact NDT Systems Employing Piezoceramic Composite Transducers*, Insight, **36**(12), pp. 926-935, 1994.
[24] Pant, S., Laliberte, J., Martinez, M. & Rocha, B., *Derivation and Experimental Validation of Lamb Wave Equations for an N-layered Anisotropic Composite Laminate*, Composite Structures, **111**, pp. 566-579, 2014.
[25] Standards Committee of the IEEE Ultrasonics, Ferroelectrics, and Frequency Control Society, *IEEE Standard on Piezoelectricity*, ANSI/IEEE Std 176-1987, 1988.
[26] Kessler, S.S., Spearing, S.M. & Soutis, C., *Damage Detection in Composite Materials Using Lamb Wave Methods*, Smart Materials and Structures, **11**, pp. 269-279, 2002.
[27] Thiene, M., Khodaei, Z.S. & Aliabadi, M.H., *Optimal Sensor Placement for Maximum Area Coverage (MAC) for Damage Localization in Composite Structures*, Smart Materials and Structures, **25**(9), 095037, 2016.
[28] Salmanpour, M.S., Khodaei, Z.S. & Aliabadi, M.H., *Impact Damage Localisation with Piezoelectric Sensors under Operational and Environmental Conditions*, Sensors, **17**(5), 1178, 2017.